1521-0103/384/1/163–172$35.00
THE JOURNAL OF PHARMACOLOGY AND EXPERIMENTAL THERAPEUTICS
dx.doi.org/10.1124/jpet.122.001355
J Pharmacol Exp Ther 384:163–172, January 2023

Translational PK/PD Modeling of Tumor Growth Inhibition and Target Inhibition to Support Dose Range Selection of the LMP7 Inhibitor M3258 in Relapsed/Refractory Multiple Myeloma

Floriane Lignet, Christina Esdar, Gina Walter-Bausch, Manja Friese-Hamim, Sofia Stinchi, Elise Drouin, Samer El Bawab,[1] Andreas D. Becker, Claude Gimmi,[2] Michael P. Sanderson, and Felix Rohdich

The Healthcare Business of Merck KGaA, Darmstadt, Germany (F.L., C.E., G.W.-B., M.F.-H., S.S., S.E.B., A.D.B., C.G., M.P.S., F.R.) and EMD Serono, Billerica, Massachusetts (E.D.)

Received June 15, 2022; accepted October 3, 2022

ABSTRACT

M3258 is an orally bioavailable, potent, selective, reversible inhibitor of the large multifunctional peptidase 7 (LMP7, β5i, PSMB8) proteolytic subunit of the immunoproteasome, a component of the cellular protein degradation machinery, highly expressed in malignant hematopoietic cells including multiple myeloma. Here we describe the fit-for-purpose pharmacokinetic (PK)/pharmacodynamic (PD)/efficacy modeling of M3258 based on preclinical data from several species. The inhibition of LMP7 activity (PD) and tumor growth (efficacy) were tested in human multiple myeloma xenografts in mice. PK and efficacy data were correlated yielding a free M3258 concentration of 45 nM for half-maximal tumor growth inhibition (KC_{50}). As M3258 only weakly inhibits LMP7 in mouse cells, both in vitro and in vivo bridging studies were performed in rats, monkeys, and dogs for translational modeling. These data indicated that the PD response in human xenograft models was closely reflected in dog PBMCs. A PK/PD model was established, predicting a free IC_{50} value of 9 nM for M3258 in dogs in vivo, in close agreement with in vitro measurements. In parallel, the human PK parameters of M3258 were predicted by various approaches including in vitro extrapolation and allometric scaling. Using PK/PD/efficacy simulations, the efficacious dose range and corresponding PD response in human were predicted. Taken together, these efforts supported the design of a phase Ia study of M3258 in multiple myeloma patients (NCT04075721). At the lowest tested dose level, the predicted exposure matched well with the observed exposure while the duration of LMP7 inhibition was underpredicted by the model.

SIGNIFICANCE STATEMENT

M3258 is a novel inhibitor of the immunoproteasome subunit LMP7. The human PK and human efficacious dose range of M3258 were predicted using in vitro–in vivo extrapolation and allometric scaling methods together with a fit-for-purpose PK/PD and efficacy model based on data from several species. A comparison with data from the Phase Ia clinical study showed that the human PK was accurately predicted, while the extent and duration of PD response were more pronounced than estimated.

Introduction

Multiple myeloma (MM) is a hematologic neoplasm characterized by the proliferation of malignant plasma cells in the bone marrow. MM accounts for approximately 1% of neoplastic malignancies and 13% of hematologic neoplasms worldwide (Palumbo and Anderson, 2011). Despite the emergence of diverse therapeutic agents, MM remains a terminal disease and patients have a high unmet medical need for novel drugs offering improved efficacy and safety (Turesson et al., 2018).

M3258 has a novel, orally bioavailable, potent, highly selective, reversible inhibitor of the large multifunctional peptidase 7 (LMP7/β5i/PSMB8) subunit of the immunoproteasome (iP) (Klein et al., 2019; Sanderson et al., 2019). M3258 showed strong in vivo efficacy in preclinical MM xenograft models and an improved preclinical safety profile compared with the approved pan-proteasome inhibitors (pan-PIs) bortezomib, carfilzomib and ixazomib, which target LMP7 as well as other proteolytic subunits of the iP and constitutive proteasome (cP) (Klein et al., 2019; Sanderson et al., 2019).

Modeling of the relationships between preclinical pharmacokinetic (PK) and pharmacodynamic (PD) properties of novel

This work received no external funding. This research was supported by the Healthcare Business of Merck KGaA, Darmstadt, Germany.
All authors were employees of the healthcare business of Merck KGaA, Darmstadt, Germany or its affiliate EMD Serono Billerica, MA USA.
[1]Current affiliation: Translational Medicine, Servier, Suresnes, France.
[2]Claude Gimmi was an employee of the healthcare business of Merck KGaA, Darmstadt, Germany, during the preparation of this manuscript but has since retired.
C.E., G.W.-B, M.F.-H., and M.P.S. are inventors of the patent WO2022073994. C.E. is inventor of the patent WO2019038250.
dx.doi.org/10.1124/jpet.122.001355.
Ⓢ This article has supplemental material available at jpet.aspetjournals.org.

ABBREVIATIONS: AUC, area under the curve; BIW, twice weekly; CL, clearance; C_{max}, maximal concentration; cP, constitutive proteasome; f_u, fraction unbound in plasma; iP, immunoproteasome; IVIVE, in vitro–in vivo extrapolation; LMP7, large multifunctional peptidase 7; MM, multiple myeloma; NCA, noncompartmental analysis; pan-PI, pan-proteasome inhibitor; PBMC, peripheral blood mononuclear cell; PD, pharmacodynamic; PK, pharmacokinetic; QD, *quaque die*, once a day; r/r, relapsed/refractory; TGI, tumor growth inhibition.

anticancer agents, to predict their effects in humans has proven a pivotal approach in drug development (Mould et al., 2015; Venkatakrishnan et al., 2015; Zhou and Gallo, 2011). The relationship between inhibition of cP and iP proteolytic subunits and the antitumor efficacy of pan-PIs has been studied in preclinical species and in clinical studies. For example, ixazomib was shown to be associated with more pronounced efficacy and cP subunit inhibition in solid tumor and hematologic xenograft models compared with bortezomib (Kupperman et al., 2010). A clinical study of ixazomib in relapsed/refractory (r/r) lymphoma patients demonstrated dose-dependent inhibition of proteasome activity (Assouline et al., 2014). Finally, a clinical study with carfilzomib in MM patients indicated that proteasome subunit occupancy correlated with antitumor efficacy (Lee et al., 2016).

In this report, we describe for the first time the PK profile of M3258 across different species as well as the establishment of PK/PD/efficacy models for the prediction of the active dose range for M3258 in human. As the iP is expressed in immune cells (Boegel et al., 2018; Sijts and Kloetzel, 2011), and since the intended indication for M3258 is MM, peripheral blood mononuclear cells (PBMC) were selected for the assessment of the inhibition of LMP7 activity by M3258. The selection of PBMCs is further supported by a previous publication, which used these cells for assessment of the PD effects of the pan-proteasome inhibitor carfilzomib on LMP7 and other iP subunits (Lee et al., 2016). Importantly, it was shown previously that the inhibition of LMP7 activity by M3258 was reduced in mouse cells compared with human, rat, dog, and monkey cells (Sanderson et al., 2021). Therefore, other preclinical species were investigated to allow the establishment of a PK/PD model in PBMCs. This data and the associated modeling and simulation efforts supported the design of a phase I dose-escalation trial of M3258 in r/r MM patients (ClinicalTrials.gov identifier: NCT04075721). Finally, the accuracy of the translational models described herein was examined by comparing the predicted PK and PD to the observed human exposure and inhibition of LMP7 activity following single or repeated oral application of M3258 in r/r MM patients.

Materials and Methods

In Vitro ADME

Plasma Protein Binding. The in vitro protein binding of M3258 was investigated by equilibrium dialysis (3 hours) in human, dog, monkey, rat, or mouse plasma and in a solution of 750 μM purified human serum albumin in 70 mM phosphate buffer, pH 7, at nominal concentrations of 0.5, 5, and 50 μM for M3258 and 1 μM for the positive control ([^{14}C]-testosterone). The human plasma was sampled on April 23, 2018, at Nuvisan GmbH, Germany from 1 Caucasian female, who signed an informed consent on March 8, 2018. Mouse, rat, and dog plasma were supplied by Nuvisan GmbH, Germany, and the monkey plasma by Bioculture (Mauritius) Ltd. The concentrations of M3258 and the positive control ([^{14}C]-testosterone) were determined by ultra-high performance liquid chromatography with tandem mass spectrometric detection (UPLC-MS/MS) and liquid scintillation counting (LSC), respectively. Details of the assay procedure are provided in the Supplemental Information.

Blood to Plasma Ratio. The in vitro distribution of M3258 was investigated in fresh human, dog, monkey, rat, or mouse whole blood at concentrations of 0.5, 5, and 50 μM. Human, dog, rat, and mouse whole blood was collected by Nuvisan GmbH, Germany. The Caucasian male donor signed an informed consent the week prior to sampling. Monkey blood was provided by BioIVT, West Sussex, UK. The blood to plasma ratios were determined by UPLC-MS/MS quantification of M3258 concentrations in plasma obtained from whole blood by centrifugation following incubation for 30 minutes at 37°C as well as in control plasma, which served as a volumetric surrogate for the spiked whole blood. Details of the assay procedure are provided in the Supplemental Information.

Metabolic Stability. The in vitro metabolic stability of M3258 was investigated in cryopreserved hepatocytes from mouse, rat, dog, monkey, and human obtained from BioIVT, West Sussex, UK, at a substrate concentration of 0.25 μM. Parent drug decline up to 5 hour was quantified by UPLC-MS/MS (Supplemental Information). Unbound intrinsic clearance values (CL_{int}) in all species were derived by correcting for hepatocyte binding calculated from the logP value of M3258 using the Kilford equation (Kilford et al., 2008).

Caco-2 Permeability. The apparent permeability (Papp) coefficient, recovery, and efflux ratio data for M3258 were assessed in assays with human Caco-2 cells (TC7 clone). Cell monolayers were differentiated for a minimum of 14 day in culture prior to use. M3258 was applied at 1 μM on the donor side and analyzed by LC-MS/MS in the donor and receiver wells after incubation for 2 hours. The permeability was determined in the apical-to-basolateral (A > B) and basolateral-to-apical (B > A) directions using Hanks' Balanced Salt solution at pH 7.4 in both compartments. A detailed description of the assay procedure was described previously (Mallinger et al., 2016).

Animal Studies

All procedures in animals described in the following discussion were performed in compliance with the Animal Welfare Act(s), the recommendations of the Association for Assessment and Accreditation of Laboratory Animal Care and national Animal Health regulations. Animal protocols were reviewed by the Animal Welfare Body of the relevant test facilities; either Merck Healthcare KGaA (Darmstadt, Germany), Istituto di Ricerche Biomediche "Antoine Marxer"–RBM S.p.A. (Ivrea, Italy), or Porsolt SA. (Le Genest-Saint-Isle, France) and approved by local authorities.

In Vivo Pharmacokinetics

In Vivo PK In-Life Phase. Single application intravenous PK studies with M3258 were performed in mouse (1 mg/kg, n = 3), rat (1 mg/kg, n = 3), dog (0.2 mg/kg, n = 2) and monkey (0.3 mg/kg, n = 3). In each study, pre-application blood samples as well as multiple consecutive samples up to 24 hours postapplication were taken and used for plasma isolation.

Bioanalytics. The concentrations of M3258 in plasma were quantified using UPLC-MS/MS, as described previously in the Supplemental Information of Sanderson et al. (2021).

PK evaluation. Area under the curve (AUC), clearance (CL), volume of distribution at steady state (V_{ss}), half-life ($t_{1/2}$) and all dose-normalized values were calculated using the software Phoenix WinNonlin (Certara, L.P., Princeton, NJ, USA). AUC values were calculated by noncompartmental analysis (NCA) using the linear up/log down method.

Analysis of LMP7 activity. Cleavage of the fluorogenic peptidic substrate (Ac-ANW)2R110 was used to assess LMP7 activity ex vivo in isolated PBMCs, spleen and tumor tissue as described previously (Sanderson et al., 2021).

Translational Studies in Preclinical Species

Single Oral Application Studies. All single application experiments used M3258 suspended in 0.25% methylcellulose/0.25% Tween 20 in PBS.

A PK/PD study was performed in H2d Rag2 female mice (n = 134) bearing U266B1 xenografts, as described previously (Sanderson et al., 2021).

Female Wistar rats (n = 21) received a single oral administration of M3258 at 10 mg/kg. Rats were euthanized at 0.25, 0.5, 1, 2, 6, 24 and 48 hour after treatment (n = 3 per time point). M3258 concentrations were measured in plasma. Spleen samples were isolated for assessment of LMP7 activity, as described in the previous discussion.

Female Beagle dogs (n = 2) received a single oral administration of M3258 at 3 mg/kg. Consecutive blood samples were taken from the cephalic vein, pre-application and after 0.25, 0.5, 1, 4, 5, 6, and 24 hours and split into 2 aliquots for the assessment of the plasma concentrations of M3258 and for PBMCs isolation (4, 6, and 24 hours) for analysis of LMP7 activity.

Male Cynomolgus monkeys (n = 3) received a single oral application of M3258 at 3 mg/kg. Consecutive blood samples were taken from the femoral vein, preapplication and after 0.25, 0.5, 1, 2, 4, 6, and 24 hours and split into 2 aliquots for determination of M3258 concentrations in isolated plasma and for PBMCs isolation (4, 6, and 24 hours) for analysis of LMP7 activity.

Repeated Oral Application Studies. Wistar rats (6 animals per sex and dose group) received repeated oral administrations of M3258 (3, 10, or 30 mg/kg) suspended in 0.5% methylcellulose/0.25% Tween 20 in PBS for 14 days. Consecutive blood samples were taken before treatment and 0.25, 0.5, 1, 2, 4, 6, 24, and 48 hours after the final treatment of the determination of plasma concentrations of M3258. PBMC and spleen samples were collected from each animal in each dose group, either at 6, 24, or 48 hours after treatment and analyzed for LMP7 activity.

Two repeated application studies were performed in dogs, as follows. In the first study, M3258 was applied orally daily for 14 consecutive days at 3 or 10 mg/kg suspended in 0.5% methylcellulose/0.25% Tween 20 in PBS to Beagle dogs (1 male and 1 female). In the second study, M3258 was applied orally daily for 28 consecutive days at 0.75, 1.5, or 3 mg/kg, suspended as in the first study, to 3 male and 3 female Beagle dogs. Blood samples were taken before treatment and 0.25, 0.5, 1, 2, 6, 10, and 24 hours after treatment on the first day for both studies and on day 25 of the second study. Samples were separated into 2 aliquots for assessment of M3258 concentrations in isolated plasma and for PBMCs isolation (6 and 24 hours) for analysis of LMP7 activity.

PK/Efficacy Studies in Mouse Xenograft Models. In vivo efficacy studies were conducted using H2d Rag2 female mice xenografted with human U266B1 MM cells, as described previously (Klein et al., 2021; Sanderson et al., 2021). Tumor growth inhibition (TGI) by M3258 was examined in a first study using the oral doses of 0.1, 0.3, and 1 mg/kg daily (QD) and 1 mg/kg either QD, Q2D (once every 2 days), or twice weekly (BIW) in a second study. Both studies included a group treated with vehicle. Animals were euthanized by an overdose injection of chemical anesthetics Ketamine/Xylazine followed by cervical dislocation.

Modeling and Simulation

All in vivo and ex vivo data (PK, PD, and tumor xenograft volumes) were analyzed and modeled sequentially using the Phoenix platform (Certara, L.P., Princeton, NJ, USA) containing WinNonlin 6.4 and NLME 1.2. PK/PD simulations were performed using the same platform.

PK Modeling. The mouse M3258 PK data from single- and repeated-application studies were described by a 1-compartment PK model, while the PK data from single- and repeated-application studies in rat, dog, and monkey were described by 2-compartment PK models. For each species, the model parameters were estimated using the naïve pooled engine implemented in Phoenix, based on a quasi-Newton algorithm. The obtained PK parameters were used to simulate the M3258 plasma concentrations for the establishment of the PD model.

PD Modeling. The percentage inhibition of LMP7 activity by M3258 relative to control in human MM tumor xenografts in mice and rat spleens and in PBMCs from dog and monkey were calculated and used as ex vivo PD response readouts (noted as E in equations) for the establishment of PK/PD models in each preclinical species. The tumor, rat spleen and dog PBMC PD data were described using an I_{max} model, as outlined in Eq. (1):

$$E = E0 - \frac{I_{max} \times C}{C + IC_{50}} \quad (1)$$

C is the total plasma concentration of M3258, $E0$ represents baseline LMP7 activity, I_{max} indicates the maximum percentage decrease of LMP7 activity, and IC_{50} refers to the M3258 plasma concentration resulting in half-maximal inhibition of LMP7.

Efficacy Modeling. A TGI model adapted from a previous report (Jumbe et al., 2010) was fitted to the tumor volume data from the U266B1 xenograft studies using repeated application of M3258. This tumor cell kill model describes different states of dying tumor cells, represented by a series of compartments. Equations 10 to 13 (Jumbe et al., 2010) were used in this model. The addition of a term of decrease over time λ to the inhibitory effect of the drug $S(C)$ is outlined below in Eq. (2), as described previously (Claret et al., 2009).

$$S(C) = \frac{K_{max} \cdot C}{KC_{50} + C} \times e^{-\lambda \cdot t} \quad (2)$$

Interindividual variability for the parameters describing the initial tumor size (TV0) and the tumor growth rate (K_g) were included in the model to account for the differences observed between the 2 experimental data sets. All other parameters relative to the antitumor effect of M3258 were set constant across individuals.

Human PK and Dose Prediction. The prediction of the human CL of M3258 was performed using the following approaches:

- Allometric scaling of in vivo i.v. M3258 PK in mouse, rat, dog, and monkey corrected by fraction unbound in plasma (fu), blood to plasma ratios and unbound intrinsic clearance (NASfu), in keeping with a previously described method (Lave et al., 1999).
- Simple allometric scaling normalized by protein binding (SAfu) as described previously (Ring et al., 2011).
- The Tang-Mayersohn equation, based on allometric scaling and the ratio between human and rat fu (Tang and Mayersohn, 2005).
- Allometry by rule of exponents as described previously (Mahmood and Balian, 1996), using in vivo M3258 intravenous data from mouse, rat, dog, and monkey and corrected for maximum life span (SAfu/MLP).
- In vitro–in vivo extrapolation (IVIVE) using intrinsic clearances (CL_{int}) values based on human hepatocyte data (Poulin et al., 2012).

The prediction of the human V_{ss} for M3258 was performed using the following approaches:

- Simple allometry from intravenous M3258 PK studies in mouse, rat, dog, and monkey, corrected by fraction unbound in plasma (Jones et al., 2011).
- The Øie–Tozer method, using physiologic constants described previously (Obach et al., 1997).
- Human–dog proportionality as defined by Eq. (3):

$$V_{hu} = V_{dog} \times {}^{f_{u,hu}}/_{f_{u,dog}} \quad (3)$$

Additionally, the CL, V_{ss}, fraction absorbed (fa) and rate of absorption were derived from physiologically based pharmacokinetic simulations using GastroPlus with the following input parameters: physicochemical parameters, solubility, permeability, fraction unbound, and blood-

to-plasma ratios. The oral bioavailability of M3258 was estimated using the following equation:

$$F=(1-CL/Qh)\ x\ fa. \quad (4)$$

The human oral PK profiles for M3258 were simulated using a 1-compartment PK model and PK parameters were calculated by NCA as described in the previous discussion. The M3258 daily dose yielding an average free exposure similar to the mouse efficacious exposure was computed using Eq. (4):

$$Dose=\frac{AUC \times CL \times \tau}{F} \quad (5)$$

The dosing interval τ was set to 24 hours for the computation of daily doses.

The human biologically efficacious dose range was estimated considering a 2-fold uncertainty for the clearance prediction and accounting for the know uncertainty of the clearance prediction methods.

The inhibition of LMP7 activity by M3258 in human PBMCs was simulated using the dog PK/PD model, with the PK portion replaced by the predicted human PK parameters.

Phase I Dose Escalation Study

This study (ClinicalTrials.gov identifier: NCT04075721) was designed to determine the safety, tolerability, pharmacokinetics, pharmacodynamics, and early efficacy signs of M3258 as single agent in patients with r/r MM.

This study was conducted in accordance with the protocol and consensus ethical principles derived from international guidelines including the Declaration of Helsinki, CIOMS International Ethical Guidelines, applicable ICH GCP Guidelines, applicable laws and regulations. The trial was reviewed and approved by an Institutional Review Board (IRB; for United States) and Comités de Protection des Personnes (CPP; Ethics Committee for France) before the study was initiated. All amendments to the protocol were approved by IRB/CPP before implementation of changes to the study design.

Participants signed the informed consent that met the requirements of 21 CFR 50, local regulations, ICH guidelines, HIPAA requirements, where applicable, and the IRB/CPP or study center before enrollment in the clinical study.

Blood was sampled before administration, and at 1, 2, 3, 4, 5, 6, 8, and 24 hours after the first dose, on day 1 of cycle 1 (C1D1), and before application and at 1, 2, 3, 4, 5, and 6 hours after administration on day 15 of cycle 1 (C1D15).

Within 30 minutes of collection, blood samples were centrifugated at 4°C and 1500 *g* for 10 minutes to generate plasma. Plasma (100 μL) was then added to 100 μL of 22% formic acid before being frozen at −80°C. The PK bioanalysis was performed as described previously (Sanderson et al., 2021).

PBMC Isolation and LMP7 Activity Assay. For PD evaluations, PBMCs were collected before administration of M3258 and at 2, 6, and 24 hours after the first dose on C1D1, as well as before administration and 2 and 6 hours after administration on C1D15.

Human whole blood samples from patients were collected in Na-citrate CPT (BD, Franklin Lakes, NJ, USA) and PBMCs isolated according to manufacturer's instructions with the modification of a red blood cell lysis step (Miltenyi Biotec, Bergisch Gladbach, Germany) performed before the cell washing step. Cells (n = 100,000), resuspended in 100 μL of Dulbecco's PBS (Gibco, Grand Island, NY, USA), were seeded per well and 50 μL of Proteasome-Glo cell-based buffer (Promega, Madison, WI, USA) supplemented with (Ac-ANW)2R110 substrate (AAT Bioquest, Sunnyvale, CA, USA) at a final concentration of 10 μM added to each well. Plates were shortly shaken, incubated for 30 minutes at 37°C and then centrifuged at *300 g* for 3 minutes. Fluorescence at excitation 485 nm and emission 535 nm was measured, and percent residual activity from baseline was plotted for each patient sample.

PK samples were available from 1 patient from cohort 1, treated with 10 mg QD of M3258, and 3 patients from Cohort 2, treated with 10 mg BIW of M3258, while PD data were available from 1 patient from cohort 1 and 2 patients from cohort 2.

Results

In Vitro ADME and In Vivo PK and PD Profiles

M3258 is characterized by a favorable and consistent ADME profile across different preclinical species, exemplified by high metabolic stability, low in vivo CL (0.2–0.4 L/h/kg, i.e., 3%–13% of the liver blood flow), low to moderate volumes of distribution (0.4–1 L/kg) and reasonable unbound fractions in whole plasma (fu = 2.5%–14% free drug) and blood-to-plasma ratios (0.7–1) (Table 1). Human serum albumin was identified as main binding component in human plasma with a fu value of 1.83%, close to that determined in human whole plasma. Meanwhile, no dependency at the therapeutic relevant concentration level of M3258 was detected. Furthermore, the predicted in vivo CL values extrapolated from in vitro intrinsic CL data were within a 2-fold range of the observed in vivo CL values (Fig. 1A), suggesting that in vitro human CL data could be used for accurate modeling of the human PK properties of M3258. M3258 was cleared primarily in the liver via CYP450-mediated metabolism and excreted to a low extent (<5%) in urine and feces, thus supporting the reasonable IVIVE based on in vitro hepatocyte data.

The oral bioavailability and rapid absorption of M3258 in preclinical species was determined to range between approximately 30% (dog) and 100% (mouse), which is in line with the low CL, moderate to high passive permeability in Caco-2 cells (10.7×10^{-6} cm/min) and high solubility (1.97 mg/mL in water, pH 7.4).

A significant inhibition of LMP7 activity by M3258 was measured in human xenograft tissue, PBMCs from dogs and monkey and in spleen tissue from rat. The PBMCs samples from rat were not able to be analyzed, due to technical issues during sample shipment and handling.

TABLE 1
M3258 in vitro and in vivo parameters used for the allometric scaling of clearance.

Species	Plasma protein binding f_u ± SD (%)	V_{ss} (L/kg)	Plasma CL (L/h/kg)	Blood-to-plasma ratio (C_B/C_P)	Hepatocyte CL_{int} (free) (μL/min/10^6 cells)
Mouse	4.00 ± 0.09	0.47	0.19	0.68	4.0
Rat	4.51 ± 0.29	0.45	0.37	0.89	3.8
Monkey	13.5 ± 0.5	0.95	0.34	1.09	1.1
Dog	2.52 ± 0.21	0.38	0.031	0.76	0.68
Human	2.69 ± 0.07	0.28[a]	0.033[a]	0.70	<0.6

[a]Predicted.

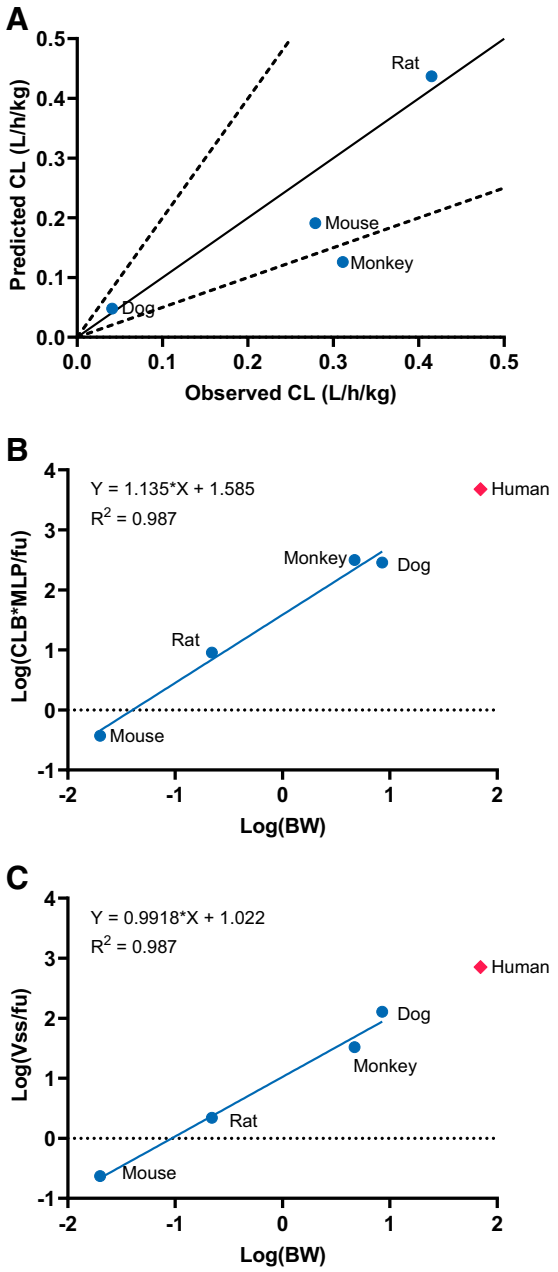

Fig. 1. Scaling approaches for the prediction of M3258 human CL and V_{ss}. (A) In vitro to in vivo correlation of M3258 total blood clearance from preclinical species. (B) Prediction of M3258 human total blood CL based on SAfu/MLP (4-species allometry corrected by maximum life span and fraction unbound). The correlation coefficient of the linear regression (R^2) was 0.987. (C) Prediction of M3258 human V_{ss} based on SAfu (4 species allometry corrected by fraction unbound). The correlation coefficient of the linear regression (R^2) was 0.987.

Preclinical PK/PD/Efficacy Modeling

PK Modeling. Plasma concentration-time courses of M3258 after oral administration in mouse were adequately described by a 1-compartment model. The model established from the single M3258 application data were validated by comparing simulations with the observations after repeated applications (Supplementary Fig. 1). The M3258 PK parameter estimates are shown in Table 2.

Plasma concentration-time courses of M3258 after oral administration in rat, dog, and monkey were adequately described by 2-compartment models. The PK parameters estimated for each species are shown in Table 2.

TABLE 2
Estimates (with CV%) of the 1- and 2-compartment M3258 PK models in mouse, rat, dog, and monkey.

Parameter	Mouse	Rat	Dog	Monkey
Ka (1/h)	2 (0)	1.3 (40)	2.6 (18)	11.6 (64)
CL/F (mL/h/kg)	146 (12)	1519 (14)	126 (10)	933 (6)
V/F (mL/kg)	849 (8)	414 (162)	552 (11)	2079 (9)
CL2/F (mL/h/kg)	—	3367 (39)	117 (7)	110 (48)
V2/F (mL/kg)	—	12808 (19)	672 (19)	1316 (59)

PK/Efficacy Modeling. The TGI model adequately captured the individual tumor growth curves observed following repeated M3258 administration in 2 separate efficacy studies using the human MM U266B1 xenograft model (Fig. 2; Supplementary Fig. 2). A time-dependent attenuation term, as described previously (Claret et al., 2009), was required to capture the apparent tumor regrowth during treatment and permit a good fit of the model to the data. The KC_{50} value of M3258 was estimated to be 370 ng/mL (44.9 nM free drug). The interindividual variability values for initial tumor volume and tumor growth rate were estimated at 26% and 33%, respectively (Table 3). Plots of the model fitting per group and diagnostic plots are shown in Supplementary Figs. 3 to 5.

PD Modeling. For each data set from human MM xenograft tumors in mice, rat spleens, and dog and monkey PBMCs, various mathematical models describing the relationship between plasma exposure and LMP7 inhibition were investigated [Emax, sigmoidal Emax, and indirect response models (Meibohm and Derendorf, 1997)]. It was found that the percentage of inhibition of LMP7 activity between treated and nontreated animals measured in human U266B1 xenografts in mice, rat spleen, and dog PBMCs could be adequately described by inhibitory I_{max} models (Figs. 3 and 4; Supplementary Fig. 6). In contrast, although a strong and prolonged inhibition of PD was observed in monkey PBMCs ex vivo, no mathematical model could adequately describe the relationship between PK and PD, due to the sparsity of the data (only 1 dose tested and 3 time points for the PD). Plots of the model fitting per group and diagnostic plots can be found in Supplementary Figs. 7 to 9. The values of the estimated parameters for each species are presented in Table 4. In dogs, the M3258 IC_{50} for LMP7 inhibition was estimated at 120 ng/mL total drug (9.1 nM free drug) with a maximal LMP7 inhibition of 81%. The estimated IC_{50} values were also expressed as free drug concentrations and were comparable to previously reported in vitro cellular LMP7 inhibition (IC_{50}) values for M3258 [Table 5 (Sanderson et al., 2021)]. The IVIV correlation for human tumor cells (U266B1) and rat PBMCs was within 2-fold. A more pronounced, yet still acceptable, 4-fold difference was observed between the IC_{50} values derived from in vivo and in vitro analyses with dog PBMC.

The maximal inhibition estimates across species were in the range of 50% to 80% (Table 4) and were in line with the in vitro maximal inhibition values previously reported for M3258 in cells from the corresponding species (Sanderson et al., 2021).

The PK/PD model developed from the U266B1 human tumor xenograft data were used to simulate the in vivo

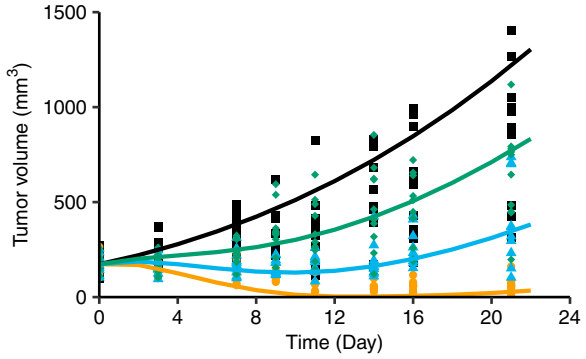

Fig. 2. Simulated and observed tumor volumes. Observed and model-fitted tumor volumes in U266B1 xenograft tumor-bearing mice treated with or without M3258 (p.o.). Lines represent model fitted tumor volumes and points indicate observed tumor volume data. Black line and black squares: control group; green line and green diamonds: M3258 0.1 mg/kg QD; blue line and blue triangles: M3258 0.3 mg/kg QD; orange lines and orange circles: M3258 1 mg/kg QD.

inhibition of LMP7 activity at different M3258 doses (Fig. 5). These simulations showed that a PD_{max} of 50% residual LMP7 activity, maintained for 6 hours, was associated with the 1 mg/kg QD dose of M3258, which delivered complete regression of human U266B1 xenograft tumors in mice. Simulations of the 10 mg/kg QD dose of M3258 showed more prolonged LMP7 inhibition.

To select the most appropriate preclinical species for translational modeling, an overlay of the PD response curves was generated from ex vivo tissue data in different preclinical species and compared with the response curve observed in the human tumor model U266B1 in mouse (Fig. 6).

Human PK, PD, and Dose Prediction

Several allometric approaches as well as in vitro scaling were used to predict the human PK characteristics of M3258 (Supplementary Tables 1 and 2). The IVIVE of in vitro CL_{int} values based on hepatocyte data from all tested preclinical species is shown in Fig. 1A. Allometric scaling of in vivo M3258 CL and V_{ss} data obtained from mouse, rat, dog, and monkey PK studies showed a reasonable extrapolation of both parameters to human (Fig. 1B and 1C). The mean values of all scaling methods were used for the calculation of the human M3258 CL and V_{ss} values at 0.033 ± 0.016 L/h/kg and 0.28 ± 0.10 L/kg, respectively (Tables 1; Supplementary Tables 1 and 2). Applying physiologically based pharmacokinetic modeling using Gastroplus, the human oral bioavailability and absorption rate of M3258 were estimated to be 80% and 0.29 $hour^{-1}$, respectively. These values were subsequently used to predict the human M3258 exposure profile.

The efficacious daily exposure for M3258 was estimated from the human U266B1 xenograft model data, as well as human MM.1S xenograft data described previously (Klein et al., 2021; Sanderson et al., 2021). The efficacious AUC range across xenograft models was calculated to be 6.8 to 18.3 μg*h/mL. Oral daily M3258 doses of 17 to 45 mg were predicted to achieve this M3258 exposure range in human, considering an average body weight of 60 kg. To account for potential uncertainties in the human clearance prediction based on in vitro and in vivo preclinical data (Yamagata et al., 2017), a 2-fold factor was included in the human dose prediction, leading to a predicted human M3258 biologically effective dose range of 10 to 90 mg per day.

The M3258 exposure was measured at C1D1 and C1D15 in 1 patient treated with 10 mg QD and in 3 patients treated with 10 mg BIW and was compared with the exposure predicted from the human PK parameters obtained using the allometric and in vitro scaling approaches (Fig. 7). An overlay of observed and predicted human exposure for both the once daily and the BIW regimens at C1D1 and C1D15 is presented in Fig. 7. Similarly, an overlay of observed and predicted LMP7 activity in patients treated with 10 mg of M3258 either once daily or BIW is presented in Fig. 8. The measured exposure was predicted accurately while the PD effect was underpredicted based on the available data.

Discussion

The prognosis for MM patients has significantly improved as a result of the emergence pan-PIs (Schlafer et al., 2017). However, this nonselective class of agents is associated with a relatively narrow therapeutic index and the development of resistance is inevitable (Wallington-Beddoe et al., 2018). As such, novel agents with selectivity for the iP, such as M3258, are of interest for application in MM patients and potentially other diseases (Ettari et al., 2018). In this report, we present the fit-for-purpose descriptive PK/PD and PK/efficacy models that were established to support the design of the recently initiated phase I study of M3258 in MM patients.

Considering the inherent differences between the bone marrow tumor environment of human MM and subcutaneous mouse xenograft tumor models (Rossi et al., 2018), translation of tumor growth characteristics from the mouse model to human MM was not attempted. Instead, efficacy predictions were performed based on M3258 plasma exposure data, with the assumption that the drug distribution from blood to the target site is similar between MM xenograft models and patients. The use of the overall exposure (or AUC) as a target metric for the prediction of the human efficacious dose was supported by the good correlation between observed tumor

TABLE 3
Estimates with coefficient of variation [CV (%)] and interindividual variability of the parameters of the model describing M3258 anti-tumor efficacy in mice bearing U266B1 xenografts.

Parameter	Description	Estimate	CV (%)	i.i.v (%)
K_{max}	Maximal tumor kill rate	10	0	—
KC_{50} (ng/mL)	Concentration leading to 50% of K_{max}	370	12	—
Lambda (1/h)	Decrease of drug effect over time	0.01	8	—
K_g (1/h)	Tumor growth rate	0.03	6	33
K_{kill} (1/h)	Tumor kill rate	0.07	6	—
TV0 (mm^3)	Initial tumor volume	171	5	26

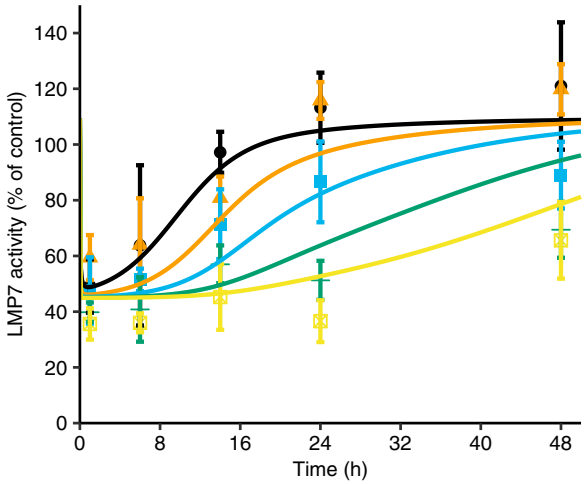

Fig. 3. Simulated and observed mouse M3258 PD profiles. Observed (points) and simulated (lines) LMP7 activity at the indicated time points in xenografted human U226B1 tumor cells in mice treated once orally with M3258 at 0.3 mg/kg (black line and circles), 1 mg/kg (orange line and triangles), 3 mg/kg (blue line and rectangles), 10 mg/kg (green line and plus symbols) or 30 mg/kg (yellow line and open squares). Data are expressed as mean ± S.D.

regression in xenograft models and AUC (Supplementary Fig. 10). The variability of M3258 sensitivity observed across different MM xenograft models (Sanderson et al., 2021) was integrated in the human dose prediction by considering the exposure at the efficacious doses in different xenograft models. This led to the estimation of a daily efficacious AUC range of 6.8 to 18.3 μg*h/mL in mice, which was predicted to be achieved at a human daily oral M3258 dose range of 10 to 90 mg.

Another objective of our study was to develop an accessible and translatable PD biomarker to monitor the inhibition of LMP7 activity by M3258 in blood in the first in-human study. Previous work showed that M3258 displayed significantly reduced in vitro inhibition of LMP7 in mouse cells, compared with its activity in human, rat, dog, and monkey cells

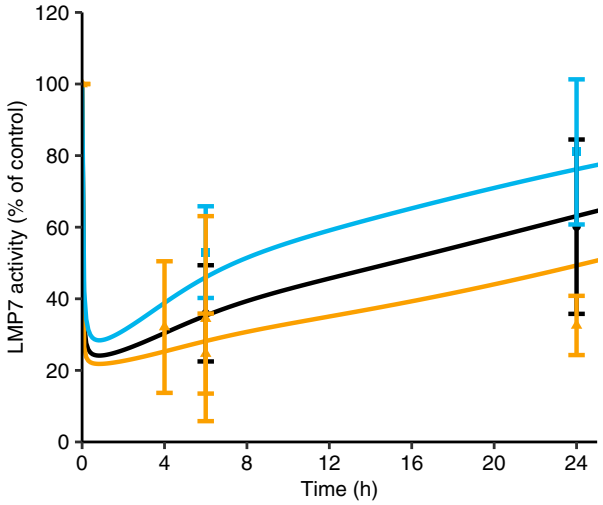

Fig. 4. Simulated and observed dog M3258 PD profiles. Observed (points) and simulated (lines) LMP7 activity at the indicated time points in PBMCs from dogs treated once orally with M3258 at 0.75 mg/kg (blue), 1.5 mg/kg (black) or 3 mg/kg (orange). Data are expressed as mean ± S.D.

TABLE 4
Estimates (and CV%) of the parameters of the PK/PD models describing LMP7 inhibition by M3258 in human U266B1 multiple myeloma xenograft tumors in mice, rat spleen, and dog PBMCs.

Parameter	MM xenograft	Rat spleen	Dog PBMCs
E0 (% of control)	109 (3)	103 (4)	100 (0.5)
I_{max} (% of control)	64 (5)	49 (10)	81 (5)
IC_{50} (ng/mL)	11 (26)	93 (38)	120 (25)

(Sanderson et al., 2021). As described previously (Huber et al., 2016; Sanderson et al., 2021) the comparable inhibitory activity of M3258 against human, rat, dog, and monkey LMP7 is likely explained by the highly conserved active site sequence of these orthologs. Meanwhile the presence of a bulky methionine-31 in the mouse LMP7 active site (valine in human, rat, dog, and monkey LMP7) results in reduced activity of selective LMP7 inhibitors in mouse cells. Therefore, in vivo PK/PD studies in rat, dog, and monkey were performed to explore the dynamic PK/PD relationship and to enable bridging of in vivo PK, PD, and efficacy data.

The overlay of PK and PD measurements in different species (Fig. 6) showed that both dog and monkey plasma PK correlated well with the exposure observed in mouse. Meanwhile, the PD in dog PBMCs most closely matched the PD in the U266B1 tumor model. In addition, the dog PK parameters derived by NCA, CL, and V_{ss}, were close to the corresponding predicted human parameters. Moreover, estimates of the PK/PD model derived from the dog data showed the lowest CV% on average. Taken together, these data supported the selection of the dog PK/PD model as the most relevant translatable PK/PD model of LMP7 inhibition for human simulations.

The variable maximal inhibition of LMP7 activity observed in different tissues (tumor, spleen, PBMCs) could potentially reflect the degree of M3258 penetration. Another explanation could be the differential expression of the iP and cP in these tissues. The substrate (Ac-ANW) 2R110 that was used in this report for assessment of LMP7 activity has been described to also undergo residual cleavage in cells by other proteasomal subunits (Sanderson et al., 2021). In keeping with this, the comparatively pronounced maximal inhibition values for M3258 in PBMCs may be explained by their dominant iP expression (Boegel et al., 2018).

The translational models of PK and PD and efficacy of M3258 from data collected in different preclinical species may not totally reflect what will be observed in patients, as clinical heterogeneity cannot be reproduced with preclinical models.

TABLE 5
LMP7 activity inhibition (IC_{50}) measured in vitro[a] in U266B1 cells and PBMCs from rat, dog, and monkey and LMP7 activity inhibition (IC_{50}) corrected for plasma protein binding obtained from PK/PD modeling of in vivo data in U266B1 cells xenografted to mouse, rat spleen tissue, and dog PBMCs, with uncertainty expressed as CV% in brackets.

Species	In vitro IC_{50} (nM)	In vivo IC_{50} (nM)
Human U266B1 cells	2	1.4 (25.8)
Rat	9.3	7.1 (37.7)
Dog	34.5	9.1 (25)
Monkey	10	ND

ND, not determined.
[a]Sanderson et al. (2021).

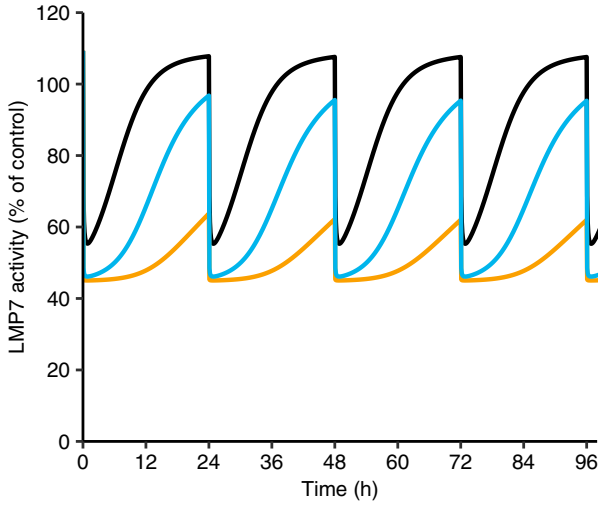

Fig. 5. Simulated PD profiles after repeated M3258 application in the U226B1 xenograft model. Simulated LMP7 activity in U266B1 xenograft tumors in mice treated orally with vehicle or M3258 at 0.1 mg/kg QD (orange), 1 mg/kg QD (blue) or 10 mg/kg QD (black).

However, it provided significant support for the early clinical development to guide the design of the first in-human study. The comparison of the human exposure at the predicted efficacious dose to the exposure in animals from pivotal toxicology studies allowed the estimation of a safe and efficacious starting dose for the first in human clinical study.

The good in vivo CL prediction based on hepatocyte data from preclinical species (within 2.5-fold) suggested that the M3258 human CL could be reasonably predicted from human in vitro data. This is further supported by the fact that M3258 predominantly undergoes hepatic clearance via CYP450 enzymes. For both clearance and volume of distribution, all scaling methods led to highly consistent values, which supported the use of the mean across all methods for calculation of the human PK parameters.

The accuracy of the predicted human M3258 PK was verified by comparing the predicted exposure with the exposure observed in patients treated either daily or BIW with 10 mg of M3258. While the sparsity of the available data prevented a precise estimation of the clearance and volume of distribution of M3258 in human, graphical comparisons suggested that the human PK was closely predicted by the selected allometry and scaling methods. The closer overlay of predicted and observed exposure after repeated M3258 application, compared with single application, may reflect the longer than expected half-life of M3258 in human. While the observed exposure at C1D1 is lower than that simulated using the predicted human PK parameters, some accumulation might lead to an exposure after repeated application, which is closer to that derived from simulations. Overall, when considering the uncertainties of human PK predictions for small molecules (Jones et al., 2011; Lombardo et al., 2013a; Lombardo et al., 2013b; Ring et al., 2011), the similarity between the observed and predicted M3258 was considered promising.

While the exposure of M3258 was reasonably predicted, LMP7 activity in human was inhibited to a more pronounced

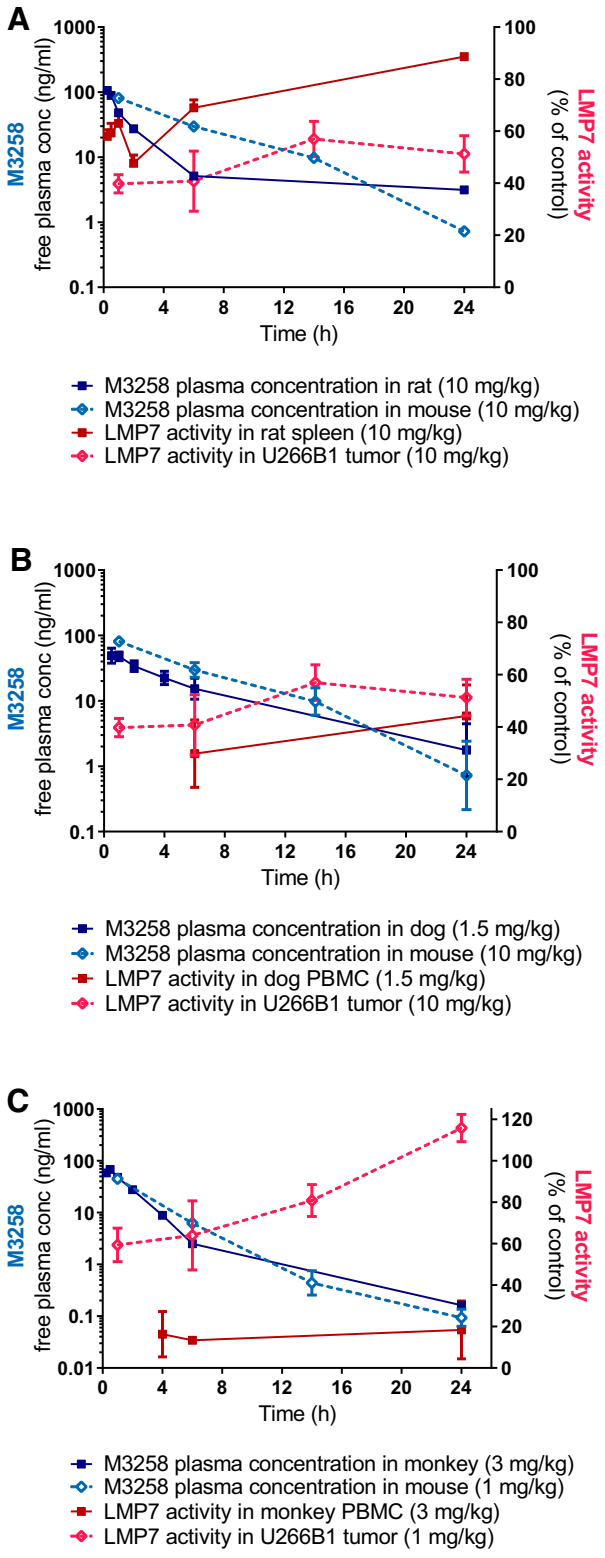

Fig. 6. Overlay of free M3258 plasma exposure (blue lines) and PD profiles (red lines) in the following models. (A) Xenografted human U266B1 tumor cells in mice treated with 10 mg/kg and in spleen tissue from rats treated with 10 mg/kg. (B) Xenografted human U266B1 tumor cells in mice treated with 10 mg/kg and in PBMCs from dogs treated with 1.5 mg/kg. (C) Xenografted U266B1 tumor cells in mice treated with 3 mg/kg and in PBMCs from monkeys treated with 1 mg/kg.

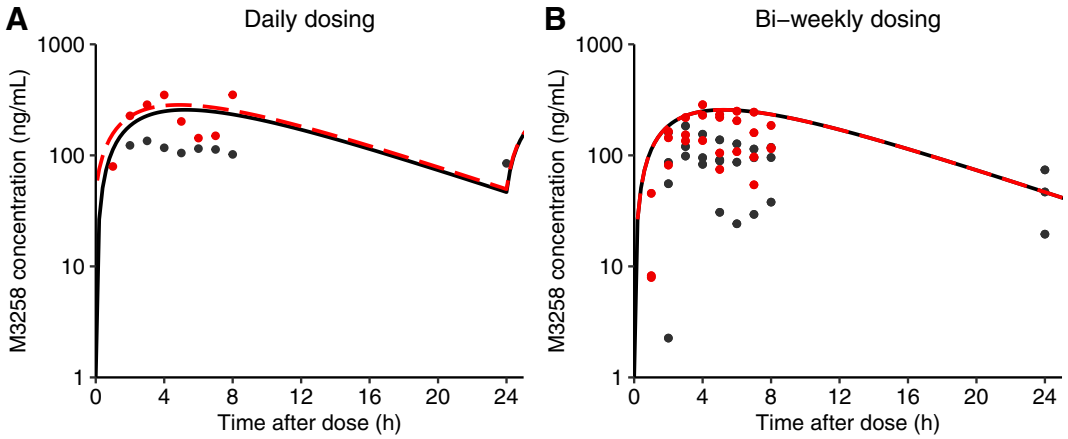

Fig. 7. Overlay of the simulated total plasma concentrations of M3258 in human as predicted using the human PK parameters obtained by scaling from preclinical parameters, and the total plasma concentrations measured in multiple myeloma patients treated with (A) 10 mg daily (cohort 1) or (B) 10 mg BIW (cohort 2). Solid black and dashed red lines: predicted exposure versus time after dose at C1D1 and C1D15, respectively; black and red points: observed exposure versus time after dose at C1D1 and C1D15, respectively.

and longer extent than anticipated from the preclinical model. Several aspects could explain the lack of accuracy of the PD prediction. At the time of the modeling, the available data supported selection of dog as the most relevant species for the establishment of a PK/PD model. The data set in monkey was limited, however somewhat mirrored the prolonged LMP7 inhibition pattern observed in human. As such, more expansive assessments (e.g., various dose levels and repeated dosing) in monkey could be performed in future studies to comprehensively assess the relevance of this species as a basis for establishment of translational PK/PD models for M3258.

Furthermore, biologic variability may lead to an inaccurate estimation of model parameters when investigating PK/PD relationships, especially when the available data are sparse (i.e., few time points and close doses). The availability of data from more time points and M3258 doses would have increased the confidence in the model estimates by enabling the use of a population approach for modeling, permitting an estimation of interindividual variability. Additionally, quantification of the inter-individual variability would have allowed inclusion of the anticipated variability in the human predictions. Finally, the longer than predicted half-life of M3258 in human could also lead to an underestimation of the duration of target engagement.

In conclusion, this work illustrates how preclinical data from different sources and different species were used to predict the human efficacious dose range of M3258. Preclinical ADME data and PK/PD modeling across different preclinical species suggested suitable properties of M3258 for application in humans. The relationship between M3258 plasma exposure and LMP7 inhibition, as well as the relationship between plasma exposure and TGI were quantitatively described by modeling. Model simulations supported the translation of M3258 from preclinical to clinical development and the design of the phase Ia dose escalation study. The human PK was reasonably predicted from the in vitro and in vivo preclinical data, while the extent and duration of LMP7 inhibition were underpredicted.

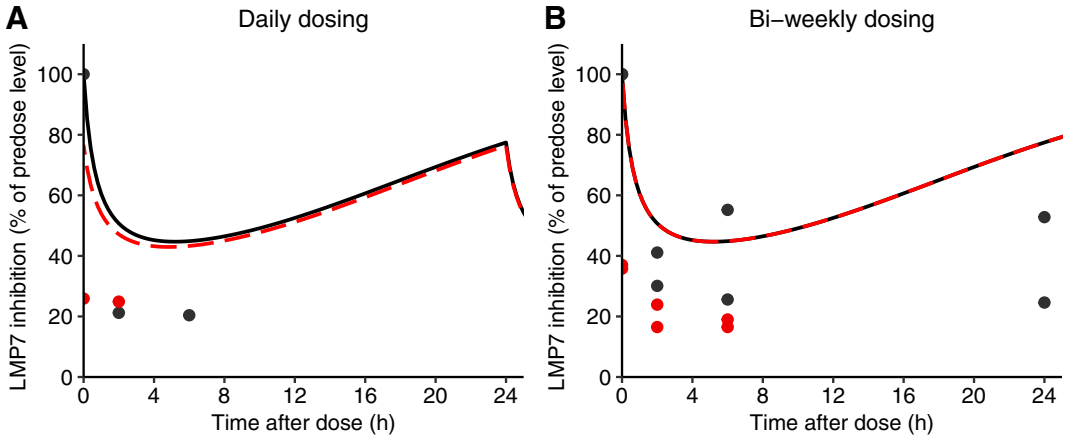

Fig. 8. Overlay of the simulated LMP7 activity in human PBMCs compared with baseline as predicted using the PK/PD model developed from preclinical data, and inhibition of LMP7 activity measured in multiple myeloma patients treated with (A) 10 mg daily (cohort 1) or (B) 10 mg BIW (cohort 2), expressed as percentage of the predose level. Solid black and dashed red lines: Predicted inhibition of LMP7 activity versus time after dose at C1D1 and C1D15 respectively; black and red points: observed inhibition of LMP7 activity versus time after dose at C1D1 and C1D15, respectively.

Acknowledgments

The authors thank the patients who participated in this clinical trial and the investigators at the individual study sites. The authors acknowledge the support and contributions of the following people: Ralf Emmerich, Eleanor Harrison-Mönch, Hendrik Hollmann, Frank Jährling, Stephanie Karl, Felix Neumann, Sheila Annie Peters, Pia Sanfelice, and Stefanie Gaus.

Authorship Contributions

Participated in research design: Esdar, Friese-Hamim, Drouin, El Bawab, Becker, Gimmi, Sanderson, Rohdich.

Conducted experiments: Esdar, Walter-Bausch, Friese-Hamim, Stinchi.

Performed data analysis: Lignet, Esdar, Rohdich.

Wrote or contributed to the writing of the manuscript: Lignet, Esdar, Walter-Bausch, Friese-Hamim, Stinchi, Becker, Sanderson, Rohdich.

References

Assouline SE, Chang J, Cheson BD, Rifkin R, Hamburg S, Reyes R, Hui AM, Yu J, Gupta N, Di Bacco A, et al. (2014) Phase 1 dose-escalation study of IV ixazomib, an investigational proteasome inhibitor, in patients with relapsed/refractory lymphoma. *Blood Cancer J* **4:**e251.

Boegel S, Löwer M, Bukur T, Sorn P, Castle JC, and Sahin U (2018) HLA and proteasome expression body map. *BMC Med Genomics* **11:**36.

Claret L, Girard P, Hoff PM, Van Cutsem E, Zuideveld KP, Jorga K, Fagerberg J, and Bruno R (2009) Model-based prediction of phase III overall survival in colorectal cancer on the basis of phase II tumor dynamics. *J Clin Oncol* **27:**4103–4108.

Ettari R, Zappalà M, Grasso S, Musolino C, Innao V, and Allegra A (2018) Immunoproteasome-selective and non-selective inhibitors: A promising approach for the treatment of multiple myeloma. *Pharmacol Ther* **182:**176–192.

Huber EM, Heinemeyer W, de Bruin G, Overkleeft HS, and Groll M (2016) A humanized yeast proteasome identifies unique binding modes of inhibitors for the immunosubunit β5i. *EMBO J* **35:**2602–2613.

Jones RD, Jones HM, Rowland M, Gibson CR, Yates JW, Chien JY, Ring BJ, Adkison KK, Ku MS, He H, et al. (2011) PhRMA CPCDC initiative on predictive models of human pharmacokinetics, part 2: comparative assessment of prediction methods of human volume of distribution. *J Pharm Sci* **100:**4074–4089.

Jumbe NL, Xin Y, Leipold DD, Crocker L, Dugger D, Mai E, Sliwkowski MX, Fielder PJ, and Tibbitts J (2010) Modeling the efficacy of trastuzumab-DM1, an antibody drug conjugate, in mice. *J Pharmacokinet Pharmacodyn* **37:**221–242.

Kilford PJ, Gertz M, Houston JB, and Galetin A (2008) Hepatocellular binding of drugs: correction for unbound fraction in hepatocyte incubations using microsomal binding or drug lipophilicity data. *Drug Metab Dispos* **36:**1194–1197.

Klein M, Busch M, Esdar C, Friese-Hamim M, Krier M, Musil D, Rohdich F, Sanderson M, Walter G, Schadt O, et al. (2019) Abstract LB-054: discovery and profiling of M3258, a potent and selective LMP7 inhibitor demonstrating high efficacy in multiple myeloma models. *Cancer Res* **79:**LB-054.

Klein M, Busch M, Friese-Hamim M, Crosignani S, Fuchss T, Musil D, Rohdich F, Sanderson MP, Seenisamy J, Walter-Bausch G, et al. (2021) Structure-based optimization and discovery of M3258, a specific inhibitor of the immunoproteasome subunit LMP7 (β5i). *J Med Chem* **64:**10230–10245.

Kupperman E, Lee EC, Cao Y, Bannerman B, Fitzgerald M, Berger A, Yu J, Yang Y, Hales P, Bruzzese F, et al. (2010) Evaluation of the proteasome inhibitor MLN9708 in preclinical models of human cancer. *Cancer Res* **70:**1970–1980.

Lavé T, Coassolo P, and Reigner B (1999) Prediction of hepatic metabolic clearance based on interspecies allometric scaling techniques and in vitro-in vivo correlations. *Clin Pharmacokinet* **36:**211–231.

Lee SJ, Levitsky K, Parlati F, Bennett MK, Arastu-Kapur S, Kellerman L, Woo TF, Wong AF, Papadopoulos KP, Niesvizky R, et al. (2016) Clinical activity of carfilzomib correlates with inhibition of multiple proteasome subunits: application of a novel pharmacodynamic assay. *Br J Haematol* **173:**884–895.

Lombardo F, Waters NJ, Argikar UA, Dennehy MK, Zhan J, Gunduz M, Harriman SP, Berellini G, Liric Rajlic I, and Obach RS (2013a) Comprehensive assessment of human pharmacokinetic prediction based on in vivo animal pharmacokinetic data, part 2: clearance. *J Clin Pharmacol* **53:**178–191.

Lombardo F, Waters NJ, Argikar UA, Dennehy MK, Zhan J, Gunduz M, Harriman SP, Berellini G, Rajlic IL, and Obach RS (2013b) Comprehensive assessment of human pharmacokinetic prediction based on in vivo animal pharmacokinetic data, part 1: volume of distribution at steady state. *J Clin Pharmacol* **53:**167–177.

Mahmood I and Balian JD (1996) Interspecies scaling: predicting pharmacokinetic parameters of antiepileptic drugs in humans from animals with special emphasis on clearance. *J Pharm Sci* **85:**411–414.

Mallinger A, Schiemann K, Rink C, Stieber F, Calderini M, Crumpler S, Stubbs M, Adeniji-Popoola O, Poeschke O, Busch M, et al. (2016) Discovery of Potent, selective, and orally bioavailable small-molecule modulators of the mediator complex-associated kinases CDK8 and CDK19. *J Med Chem* **59:**1078–1101.

Meibohm B and Derendorf H (1997) Basic concepts of pharmacokinetic/pharmacodynamic (PK/PD) modelling. *Int J Clin Pharmacol Ther* **35:**401–413.

Mould DR, Walz AC, Lave T, Gibbs JP, and Frame B (2015) Developing exposure/response models for anticancer drug treatment: special considerations. *CPT Pharmacometrics Syst Pharmacol* **4:**e00016.

Obach RS, Baxter JG, Liston TE, Silber BM, Jones BC, MacIntyre F, Rance DJ, and Wastall P (1997) The prediction of human pharmacokinetic parameters from preclinical and in vitro metabolism data. *J Pharmacol Exp Ther* **283:**46–58.

Palumbo A and Anderson K (2011) Multiple myeloma. *N Engl J Med* **364:**1046–1060.

Poulin P, Kenny JR, Hop CE, and Haddad S (2012) In vitro-in vivo extrapolation of clearance: modeling hepatic metabolic clearance of highly bound drugs and comparative assessment with existing calculation methods. *J Pharm Sci* **101:**838–851.

Ring BJ, Chien JY, Adkison KK, Jones HM, Rowland M, Jones RD, Yates JW, Ku MS, Gibson CR, He H, et al. (2011) PhRMA CPCDC initiative on predictive models of human pharmacokinetics, part 3: comparative assessment of prediction methods of human clearance. *J Pharm Sci* **100:**4090–4110.

Rossi M, Botta C, Arbitrio M, Grembiale RD, Tagliaferri P, and Tassone P (2018) Mouse models of multiple myeloma: technologic platforms and perspectives. *Oncotarget* **9:**20119–20133.

Sanderson M, Busch M, Esdar C, Friese-Hamim M, Krier M, Ma J, Musil D, Rohdich F, Sloot W, Walter G, Zanelli U, Schadt O, and Klein M (2019) Abstract DDT02-01: first-time disclosure of M3258: a selective inhibitor of the immunoproteasome subunit LMP7 with potential for improved therapeutic utility in multiple myeloma compared to pan-proteasome inhibitors. *Cancer Res* **79**(13 Suppl):DDT02-01.

Sanderson MP, Friese-Hamim M, Walter-Bausch G, Busch M, Gaus S, Musil D, Rohdich F, Zanelli U, Downey-Kopyscinski SL, Mitsiades CS, et al. (2021) M3258 is a selective inhibitor of the immunoproteasome subunit LMP7 (β5i) delivering efficacy in multiple myeloma models. *Mol Cancer Ther* **20:**1378–1387.

Schlafer D, Shah KS, Panjic EH, and Lonial S (2017) Safety of proteasome inhibitors for treatment of multiple myeloma. *Expert Opin Drug Saf* **16:**167–183.

Sijts EJ and Kloetzel PM (2011) The role of the proteasome in the generation of MHC class I ligands and immune responses. *Cell Mol Life Sci* **68:**1491–1502.

Tang H and Mayersohn M (2005) A novel model for prediction of human drug clearance by allometric scaling. *Drug Metab Dispos* **33:**1297–1303.

Turesson I, Bjorkholm M, Blimark CH, Kristinsson S, Velez R, and Landgren O (2018) Rapidly changing myeloma epidemiology in the general population: Increased incidence, older patients, and longer survival. *Eur J Haematol* DOI: 10.1111/ejh.13083 [published ahead of print]

Venkatakrishnan K, Friberg LE, Ouellet D, Mettetal JT, Stein A, Trocóniz IF, Bruno R, Mehrotra N, Gobburu J, and Mould DR (2015) Optimizing oncology therapeutics through quantitative translational and clinical pharmacology: challenges and opportunities. *Clin Pharmacol Ther* **97:**37–54.

Wallington-Beddoe CT, Sobieraj-Teague M, Kuss BJ, and Pitson SM (2018) Resistance to proteasome inhibitors and other targeted therapies in myeloma. *Br J Haematol* **182:**11–28.

Yamagata T, Zanelli U, Gallemann D, Perrin D, Dolgos H, and Petersson C (2017) Comparison of methods for the prediction of human clearance from hepatocyte intrinsic clearance for a set of reference compounds and an external evaluation set. *Xenobiotica* **47:**741–751.

Zhou Q and Gallo JM (2011) The pharmacokinetic/pharmacodynamic pipeline: translating anticancer drug pharmacology to the clinic. *AAPS J* **13:**111–120.

Address correspondence to: Floriane Lignet, Drug Metabolism and Pharmacokinetics, The Healthcare Business of Merck KGaA, Frankfurterstrasse 250, Darmstadt, 64293 Germany. E-mail: floriane.lignet@merckgroup.com

Supplemental Information

Article Title: Translational PK/PD modeling of tumor growth inhibition and target inhibition to support dose range selection of the LMP7 inhibitor M3258 in relapsed/refractory multiple myeloma

Authors: Floriane Lignet, Christina Esdar, Gina Walter-Bausch, Manja Friese-Hamim, Sofia Stinchi, Elise Drouin, Samer El Bawab, Andreas D. Becker, Claude Gimmi, Michael P. Sanderson, Felix Rohdich

Journal Title: Journal of Pharmacology and Experimental Therapeutics

Manuscript Number: JPET-AR-2022-001355

Supplemental Methods

Plasma protein binding

Human plasma was prepared from whole blood collected from one female volunteer and transferred to tubes containing EDTA as anticoagulant. Plasma from dogs (Marshall Beagle®, female), rats (Wistar Han IGS,Crl :WI(Han), female), and mice (CD-I , Crl :CDI (ICR) female) was prepared from whole blood provided by Nuvisan GmbH, Grafing, Germany and collected into tubes containing EDTA as anticoagulant. Monkey plasma (Cynomolgus, female) containing EDTA as an anticoagulant was purchased from Bioculture (Mauritius) Ltd.

All incubations were performed in triplicates in a Dianorm system. After equilibrium dialysis, the contents of both compartments of each dialysis cell containing M3258 and [^{14}C]-testosterone were transferred into brown Eppendorf tubes and LSC vials, respectively. The samples containing M3258 were acidified by dilution with 22% formic acid (FA), (Sample/FA (22%), 90:10, VIV), leading to a final sample with 2.2% FA. 20 µL aliquots were then precipitated by the

addition of an internal standard solution. Samples were incubated on a shaker at 1000 rpm for 10 min, incubated for 20 min at -20°C, and re-shaken at 1000 rpm for 10 min before centrifugation at 2180 × g (4000 rpm) for 10 min. Aliquots of the supernatant from incubation samples were diluted with Milli Q water before injection into the UPLC-MS/MS system. For [^{14}C]-testosterone, incubation sample aliquots of 300 µL of the plasma or buffer compartments were mixed thoroughly with 10 mL of Ultima GoldTM XR scintillator and were cooled prior to analysis by liquid scintillation counting (LSC). The recoveries of M3258 and [^{14}C]-testosterone in all incubations ranged from 84.1 to 102% and 96.2 to 97.1%, respectively, indicating that no relevant loss of either test item or reference compound (positive control) occurred during the experiments.

Blood to plasma ratio

Whole blood samples from all species were collected into tubes containing EDTA on the day of the study (human, mouse, rat and dog) or up to three days in advance (monkey). All blood matrices were supplemented with 5% phosphate buffer (70 nM, pH 7.4) and stored at 4°C until start of the incubations. Aliquots (237.5 µL) of human, dog, monkey, rat, and mouse whole blood, as well as control plasma (separated from the same blood samples by centrifugation), were spiked with M3258 at final concentrations of 0.5, 5, and 50 µM and incubated for 30 min at 37°C (n=3) in a light restricted laboratory. Whole blood samples were centrifuged for 2 min at ~3340 *x g* to obtain plasma. Aliquots of the plasma supernatant, as well as control plasma, were transferred into light-protected Eppendorf tubes and stabilized with 22% FA (9:1, V/V). Acidified plasma sample aliquots of 20 µL were transferred into a 96-well plate (on ice) and diluted with 130 µL of an ice-cold internal standard solution in order to precipitate the proteins. The wells were sealed and shaken for 10 min under light protection and incubated for 30 min at -20°C. Thereafter, samples were shaken again for 10 min under light protection and centrifuged at 4°C for 10 min at 2180×g. A 20 µL aliquot of the supernatant was mixed with 280 µL 0.14% FA and injected onto the UPLC-MS/MS system.

Metabolic stability

Cryopreserved hepatocytes were thawed in a water bath at 37°C, transferred to a large volume of thawing medium and centrifuged for 5 min at 100 *x g*. After careful removal of the supernatant, the cell pellet was suspended in Krebs-Henseleit buffer in order to obtain the desired cell count. Suspensions of 2 x 10^6 cells/mL without serum were incubated with M3258 at 0.25 µM in triplicate for 5 h at 37°C. Samples aliquots (18 µL) were taken at time 0 and after 0.08. 0.25, 0.5, 1, 2,3, 3.3, 3.7, 4 and 5 h. The aliquots were transferred into a 96-well-plate (on ice) and diluted with 2 µL of 22% FA and 180 µL of an ice-cold internal standard solution to lyse the hepatocytes and precipitate proteins. The wells were sealed and shaken for 10 min under light protection and incubated for 20 min at -20°C. Thereafter, samples were shaken again for 10 min under light protection and centrifuged at 4°C for 10 min at 2180 *x g*. A 40 µL aliquot of the supernatant was mixed with 60 µL Milli Q® water and injected onto the UPLC-MS/MS system. The *in vitro* intrinsic clearance was calculated from the rate of compound disappearance, and corrected for hepatocyte protein binding calculated from the compound logP (Kilford et al., 2008).

Supplemental Figures

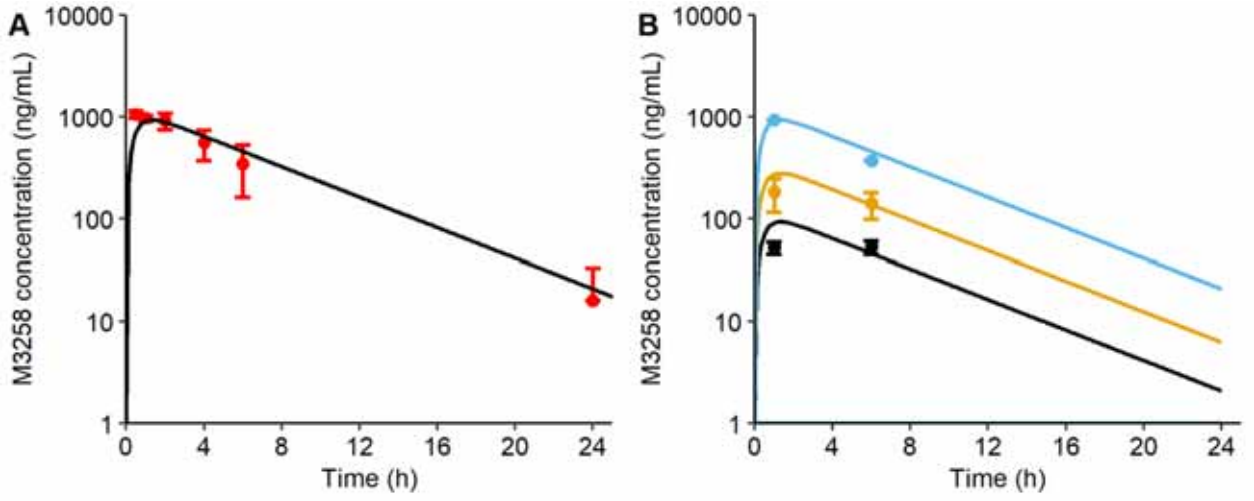

Fig. S1 Simulated and observed mouse M3258 PK profiles. **A** Observed (points) and model-fitted (lines) M3258 plasma concentrations in mice after single oral M3258 application at 1 mg/kg. **B** Mean observed (points and error bars) and model-fitted (lines) M3258 plasma concentrations in mice after repeated oral M3258 application at 0.1 mg/kg (black), 0.3 mg/kg (yellow) or 1 mg/kg (blue). Data are expressed as mean ± standard deviation

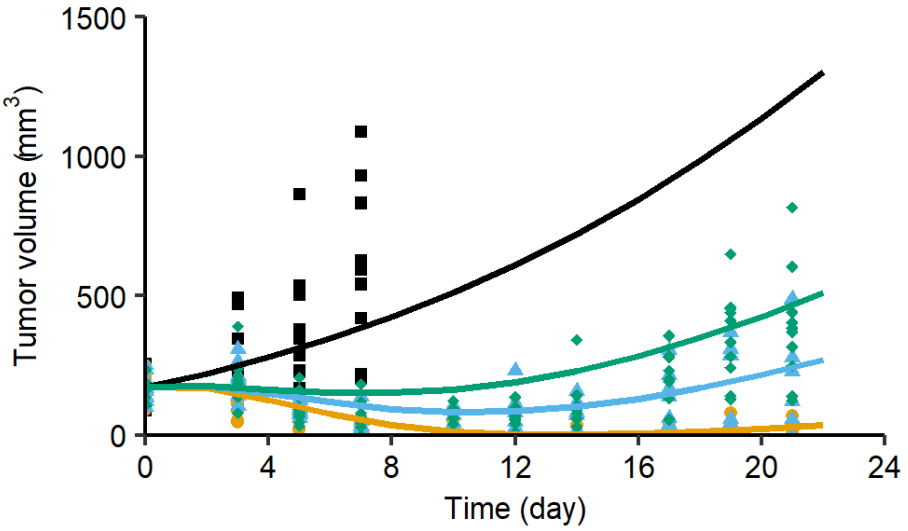

Fig. S2 Observed and model-fitted tumor volumes in U266B1 xenograft tumor-bearing mice treated with M3258 (p.o.) administered at 1 mg/kg daily (orange line and circles), once every two days (blue line and triangles) or twice weekly (green line and diamonds) or with vehicle only (black line and squares). Lines represent model fitted tumor volumes and points indicate observed tumor volume data

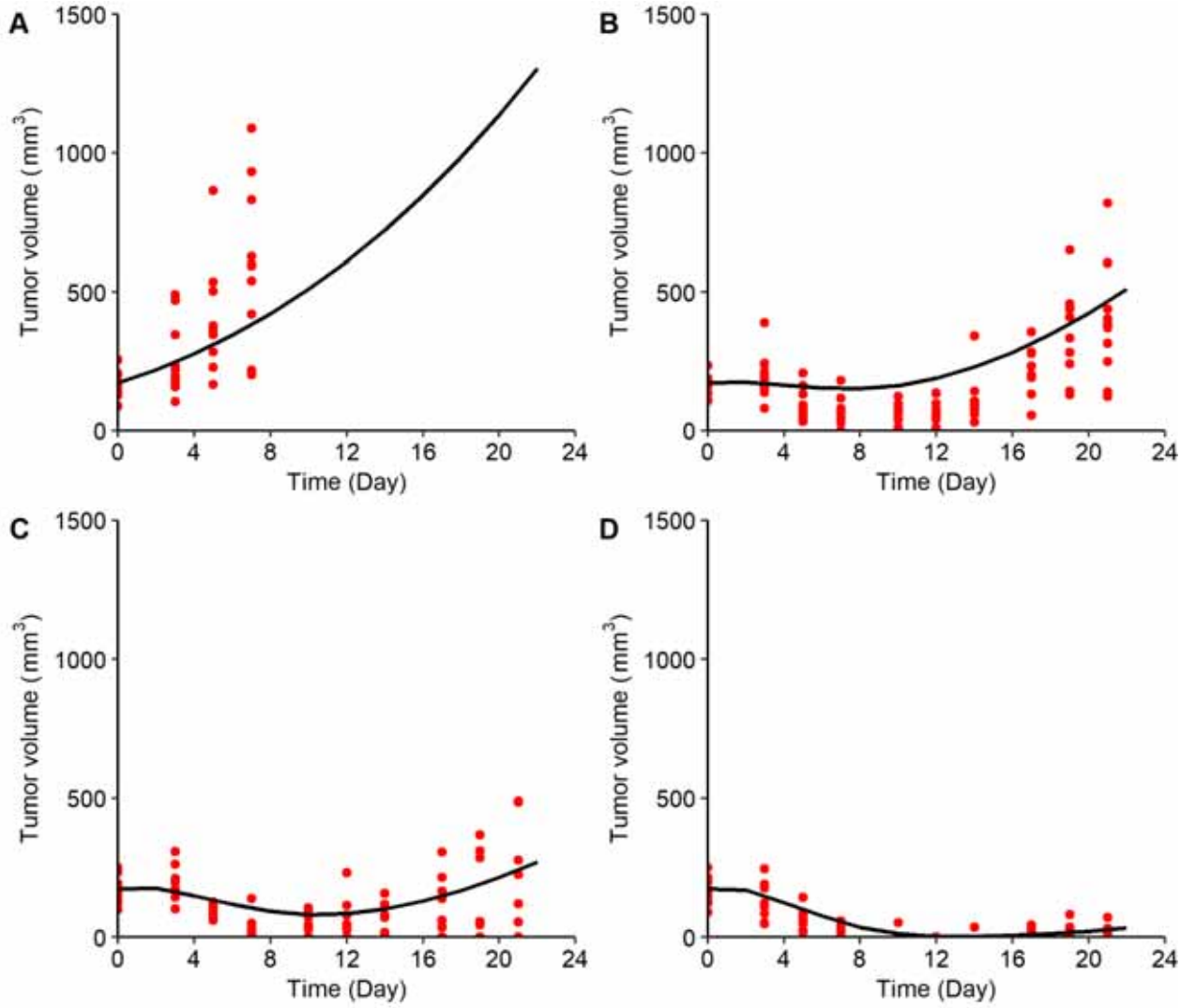

Fig. S3 Simulated and observed tumors volumes in for alternate M3258 dosing schedules. Observed (points) and model-fitted (lines) tumor volumes in U266B1 xenograft tumor-bearing mice treated orally with vehicle (**A**) or M3258 twice weekly (BIW) at 1 mg/kg (**B**), once every two days (Q2D) at 1 mg/kg (**C**) or daily (QD) at 1 mg/kg (**D**)

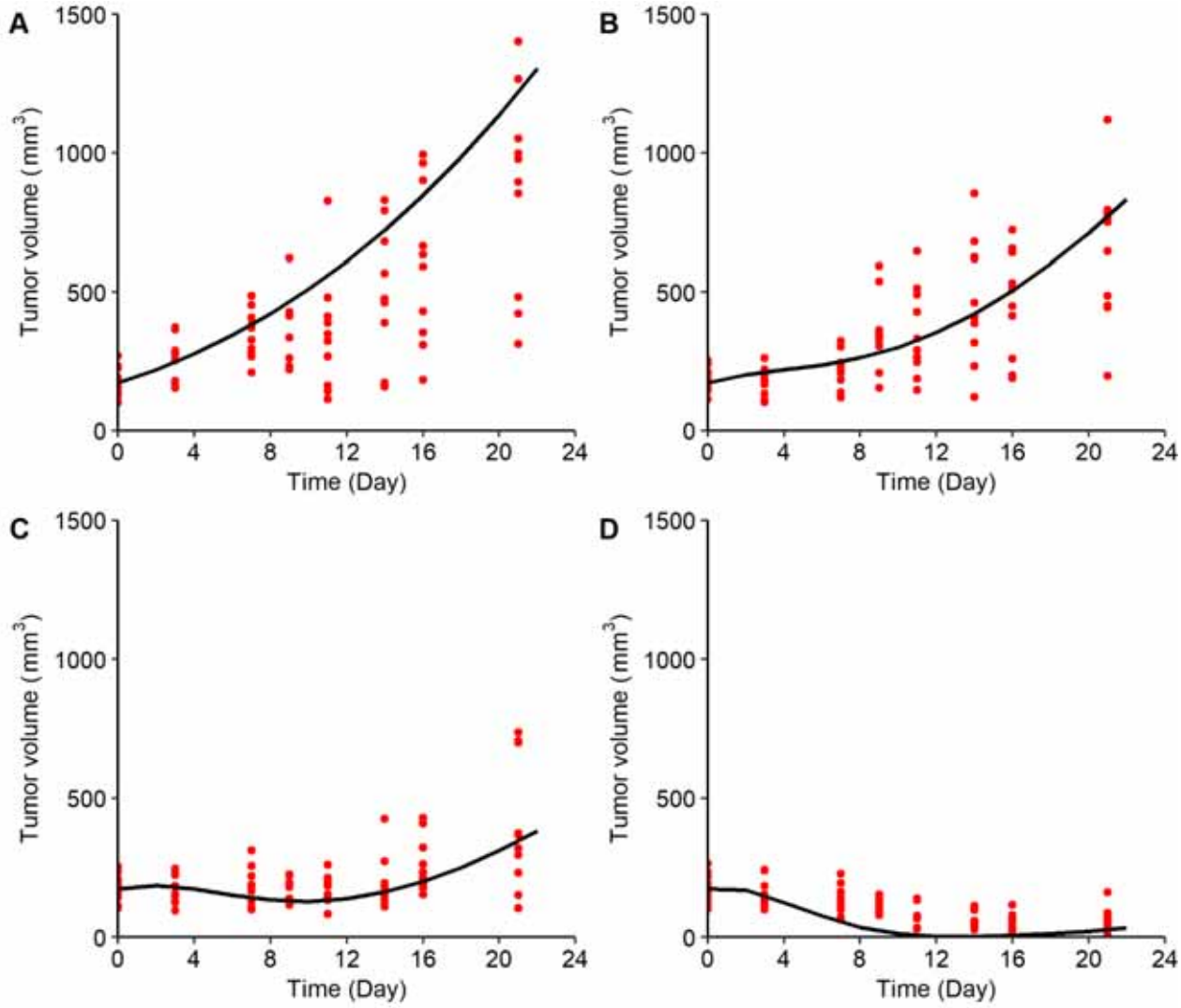

Fig. S4 Simulated and observed tumors volumes in M3258 dose range finding study. Observed (points) and model-fitted (lines) tumor volumes in U266B1 xenograft tumor-bearing mice treated orally once per day with vehicle (**A**) or M3258 at 0.1 mg/kg (**B**), 0.3 mg/kg (**C**), or 1 mg/kg (**D**)

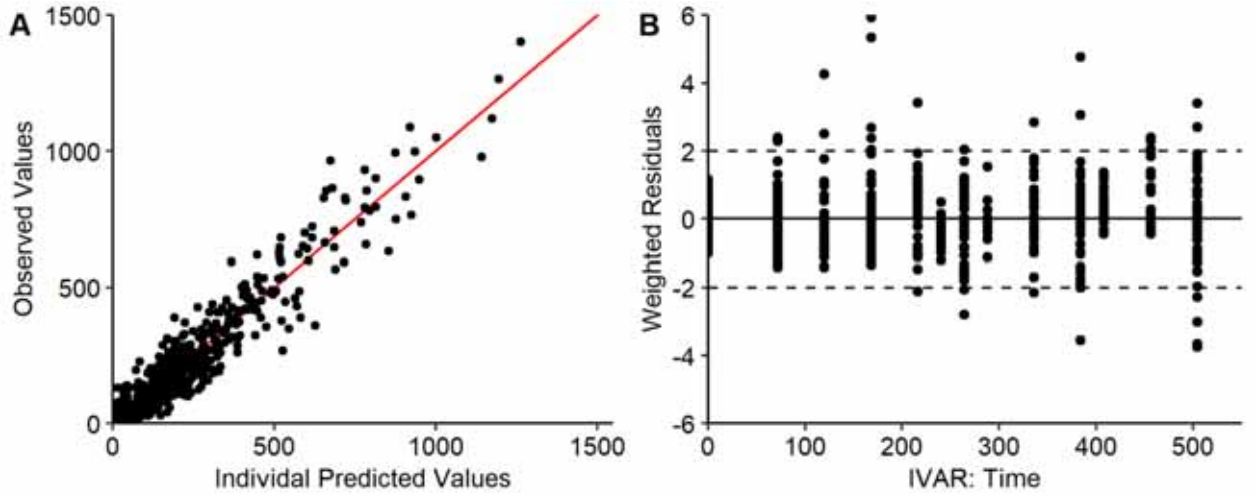

Fig. S5 Diagnostic plots for the tumor growth inhibition model. **A** Observed vs. individual predicted values (black points), overlaid with the unity line (red line). **B** Weighted residuals vs. time

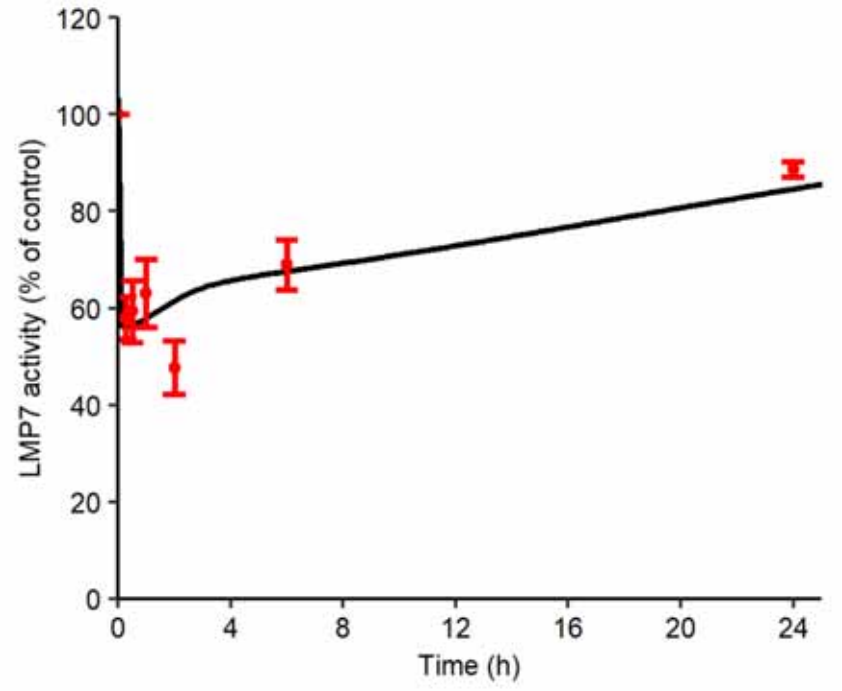

Fig. S6 Simulated and observed rat PD profile. Observed (points) and model-fitted (lines) LMP7 activity in spleens of rats treated once orally with the vehicle (black) or M3258 at 10 mg/kg. Data are expressed as mean ± standard deviation

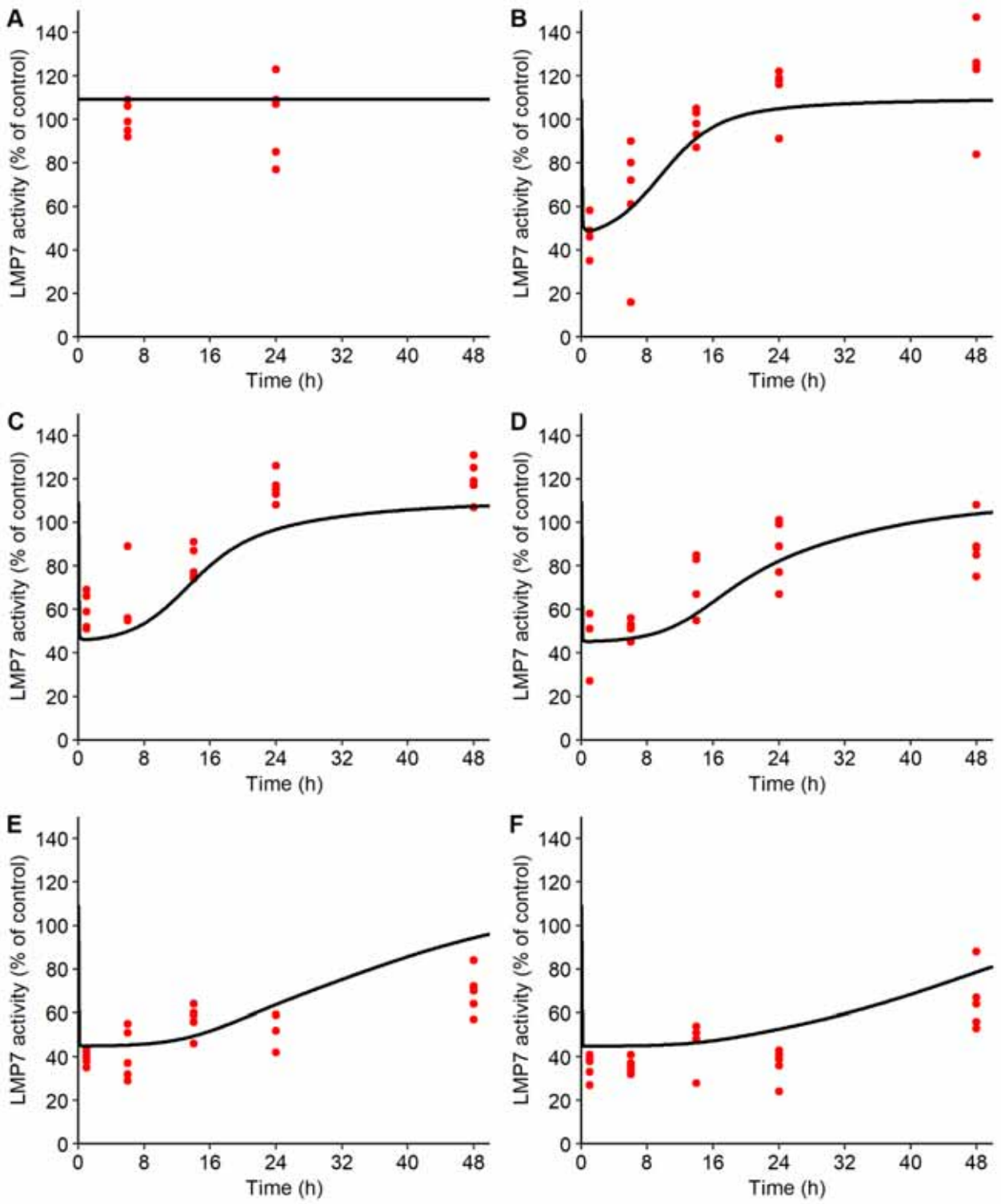

Fig. S7 Simulated and observed mouse M3258 PD profiles. Observed (points) and model fitted (lines) LMP7 activity in U266B1 xenograft tumors in mice treated orally with vehicle (**A**) or M3258 at 0.3 mg/kg (**B**), 1 mg/kg (**C**), 3 mg/kg (**D**), 10 mg/kg (**E**) or 30 mg/kg (**F**)

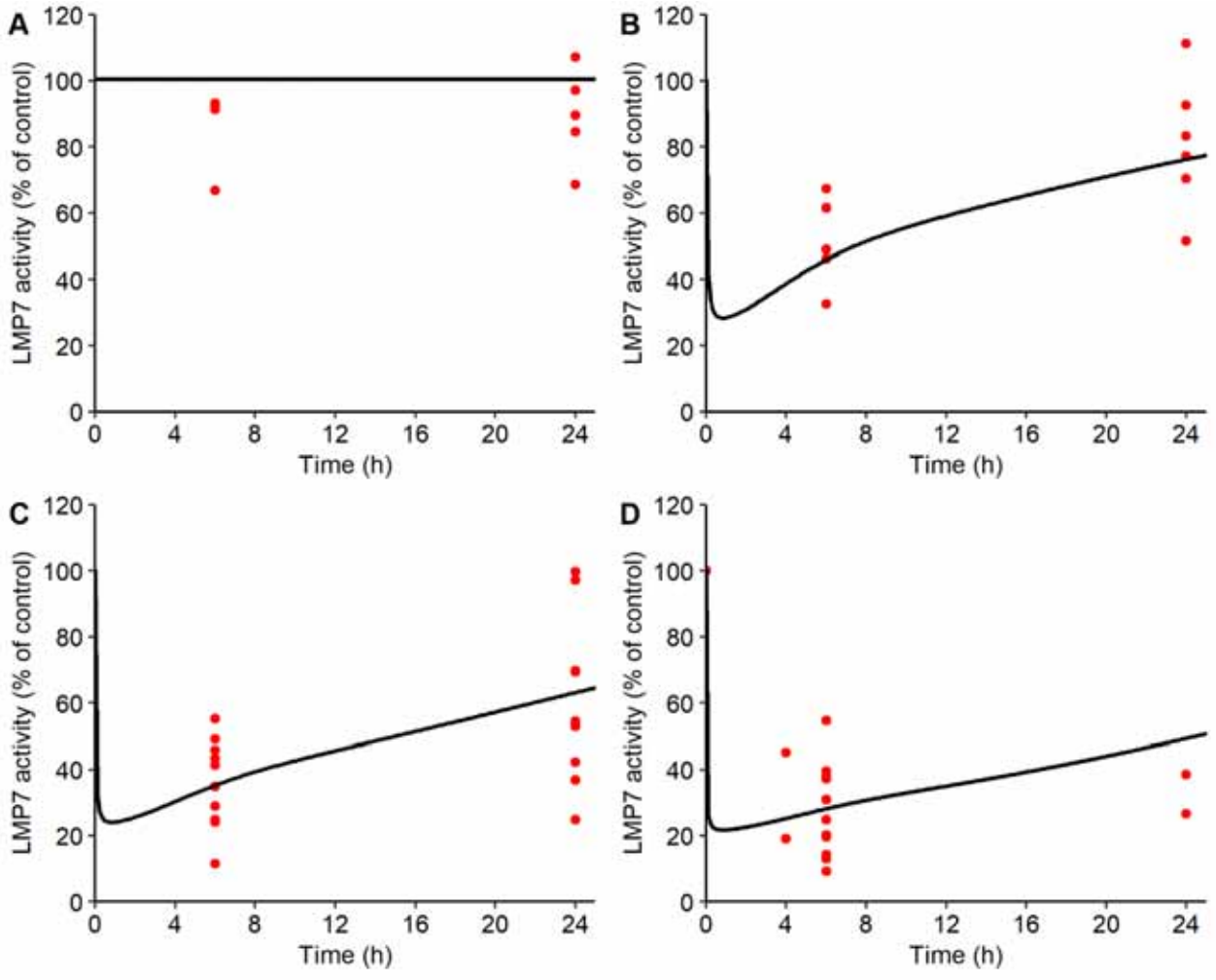

Fig. S8 Simulated and observed dog M3258 PD profiles. Observed (points) and model fitted (lines) LMP7 activity in PBMCs from dogs treated orally with vehicle (**A**) or M3258 at 0.75 mg/kg (**B**), 1.5 mg/kg (**C**) or 3 mg/kg (**D**)

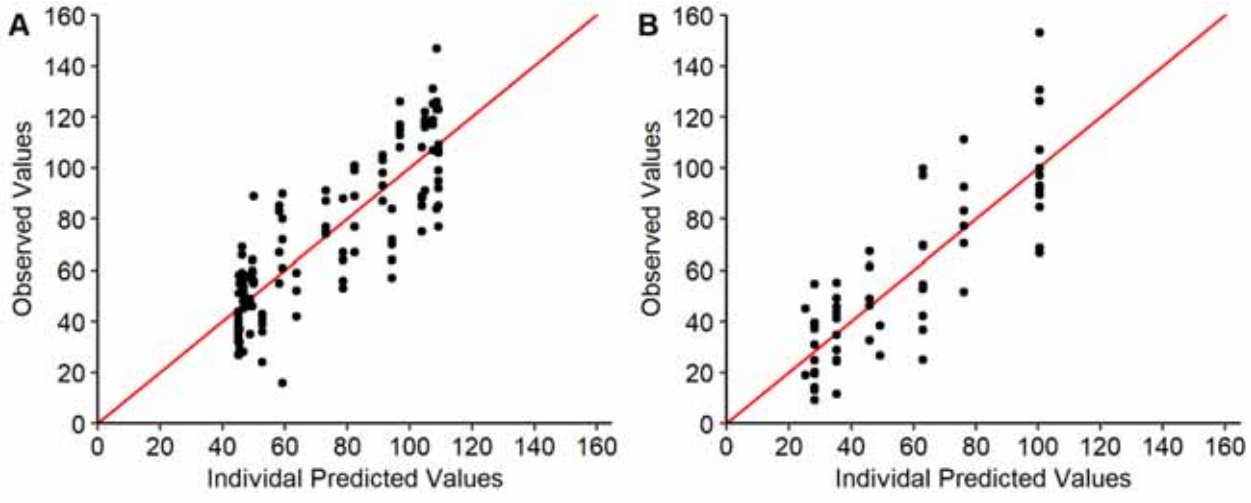

Fig. S9 Observed PD vs. PD predicted using the M3258 PK/PD models in mouse (**A**) and dog (**B**) black dots, overlaid with the unity line (red line)

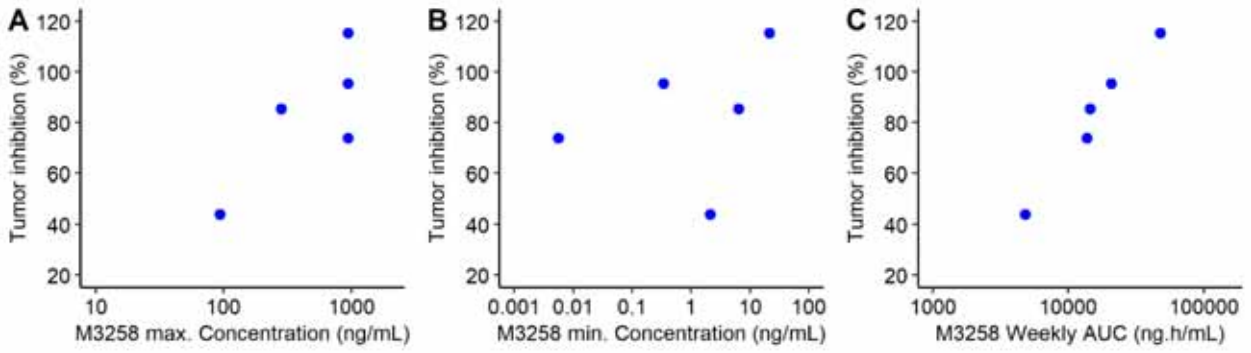

Fig. S10 Correlation between tumor growth inhibition of U266B1 xenografts in mice and C_{max} (**A**), C_{min} (**B**) and weekly AUC (**C**) of M3258 plasma exposure estimated by non-compartmental analysis.

Supplemental Tables

Table S1 Prediction of M3258 human clearance using different methods

Clearance	IVIVE	Allometric Scaling				Mean ± SD
	Regression method[a]	SAfu[b]	TME[c]	SAfu/ MLP[d]	NASfu[e]	
(L/h/kg)	<0.021[f]	0.030	0.058	0.021	0.018	0.033 ± 0.016

a: Poulin method (Poulin et al., 2012)

b: Simple allometric scaling normalized by fu (Ring et al., 2011)

c: Tang-Mayersohn-Equation (Tang and Mayersohn, 2005)

d: Simple allometric scaling normalized by fu and maximum life span (Mahmood and Balian, 1996)

e: Normalized simple allometry corrected by Clint und fu (Lave et al., 1999)

f: Clint value was below the LLOQ (0.6 µL/min/10^6 cells)

Table S2 Prediction of M3258 human volume of distribution using different methods

Volume of Distribution	SA_{fu} [a] (4-species)	Human-Dog proportionality	Øie-Tozer Method [b]	In Silico (PBPK)	Mean ± SD
(L/kg)	0.273	0.406	0.288	0.150	0.28 ± 0.10

a: Simple allometric scaling normalized by fu (Jones et al., 2011)

b: Described in Obach et al. (Obach et al., 1997)

References

Jones RD, Jones HM, Rowland M, Gibson CR, Yates JW, Chien JY, Ring BJ, Adkison KK, Ku MS, He H, Vuppugalla R, Marathe P, Fischer V, Dutta S, Sinha VK, Bjornsson T, Lave T and Poulin P (2011) PhRMA CPCDC initiative on predictive models of human pharmacokinetics, part 2: comparative assessment of prediction methods of human volume of distribution. *J Pharm Sci* **100**:4074-4089.

Kilford PJ, Gertz M, Houston JB and Galetin A (2008) Hepatocellular binding of drugs: correction for unbound fraction in hepatocyte incubations using microsomal binding or drug lipophilicity data. *Drug Metab Dispos* **36**:1194-1197.

Lave T, Coassolo P and Reigner B (1999) Prediction of hepatic metabolic clearance based on interspecies allometric scaling techniques and in vitro-in vivo correlations. *Clin Pharmacokinet* **36**:211-231.

Mahmood I and Balian JD (1996) Interspecies scaling: predicting pharmacokinetic parameters of antiepileptic drugs in humans from animals with special emphasis on clearance. *J Pharm Sci* **85**:411-414.

Obach RS, Baxter JG, Liston TE, Silber BM, Jones BC, MacIntyre F, Rance DJ and Wastall P (1997) The prediction of human pharmacokinetic parameters from preclinical and in vitro metabolism data. *J Pharmacol Exp Ther* **283**:46-58.

Poulin P, Kenny JR, Hop CE and Haddad S (2012) In vitro-in vivo extrapolation of clearance: modeling hepatic metabolic clearance of highly bound drugs and comparative assessment with existing calculation methods. *J Pharm Sci* **101**:838-851.

Ring BJ, Chien JY, Adkison KK, Jones HM, Rowland M, Jones RD, Yates JW, Ku MS, Gibson CR, He H, Vuppugalla R, Marathe P, Fischer V, Dutta S, Sinha VK, Bjornsson T, Lave T and Poulin P (2011) PhRMA CPCDC initiative on predictive models of human pharmacokinetics, part 3: comparative assessement of prediction methods of human clearance. *J Pharm Sci* **100**:4090-4110.

Tang H and Mayersohn M (2005) A novel model for prediction of human drug clearance by allometric scaling. *Drug Metab Dispos* **33**:1297-1303.